RSC Sustainability

ROYAL SOCIETY OF CHEMISTRY

PAPER

View Article Online
View Journal | View Issue

Cite this: *RSC Sustainability*, 2024, **2**, 3077

Eco-friendly synthesis and enhanced antibacterial action of bimetallic Ag/ZnO nanoparticles using *Hylocereus costaricensis* stem extract

Joel Xaviour,[a] S. Sreelekshmi,[a] Jebin Joseph,[b] S. Alfiya Fathima[c] and T. Sajini *[a]

Received 21st May 2024
Accepted 5th September 2024

DOI: 10.1039/d4su00254g

rsc.li/rscsus

This work presents a novel method for generating bimetallic silver and zinc oxide nanoparticles (Ag/ZnO-NPs) using *Hylocereus costaricensis* (HC) stem extract and microwave irradiation. Silver and zinc oxide nanoparticles were prepared separately during the synthesis process, and they were directly mixed to produce bimetallic Ag/ZnO-NPs. A thorough characterisation was conducted utilising various analytical methods to clarify the formed nanoparticles' structural, morphological and constitutional characteristics. The conventional agar well diffusion technique was then used to assess the Ag/ZnO bimetallic nanoparticles' antibacterial activity towards *Staphylococcus aureus* and *Escherichia coli*, the two most common human pathogenic bacteria. The characterisation analysis showed the successful synthesis of bimetallic Ag/ZnO-NPs with a cluster-like spherical alloy-type morphology with an average hydrodynamic diameter of 281.7 nm and a direct band gap of 2.90 eV. The antibacterial results revealed that bimetallic Ag/ZnO-NPs have a solid combinatorial antibacterial activity, underscoring their abilities to be effective antibacterial substances from renewable sources. This study opens the door for more in-depth investigation into this topic by enhancing bimetallic nanoparticles and their utilisation in the biomedical field.

Sustainability spotlight

This research exemplifies a commitment to sustainability by leveraging renewable plant extracts and energy-efficient microwave irradiation for the synthesis of bimetallic silver and zinc oxide nanoparticles (Ag/ZnO-NPs). By utilizing *Hylocereus costaricensis* stem extract, the study minimizes the environmental impact typically associated with chemical synthesis methods. The process not only reduces hazardous waste and energy consumption but also produces bimetallic nanoparticles with significant antibacterial properties, offering a green alternative for biomedical applications. This sustainable approach underscores the potential of integrating eco-friendly practices in nanotechnology, paving the way for future advancements in sustainable materials science.

1. Introduction

Nanoparticles are ultra-small particles, typically less than 100 nanometers in size, that exhibit unique physical and chemical properties due to their high surface area and quantum effects.[1] These characteristics make them highly valuable in various fields, including medicine, electronics, and environmental science.[2,3] There are several types of nanoparticles, including metallic,[4,5] metal oxide,[2] polymeric,[6,7] and carbon-based nanoparticles,[8] each with distinct features and applications.[9,10] Among the different nanoparticles, bimetallic nanoparticles are very noticeable due to the diverse characteristics of combining two different metals,[11] and they stand out due to their enhanced catalytic, optical, and antibacterial properties. These nanoparticles offer numerous advantages compared to monometallic nanoparticles, such as increased stability, better catalytic activity, and tunable surface properties.[12] The synergistic interactions between the two metals in bimetallic nanoparticles enable tailored functionality, making them particularly useful in advanced applications like catalysis, sensing, and biomedical treatments.[13,14]

Different forms of bimetallic nanoparticles, such as alloy, intermetallic, subcluster, core–shell type, and the like, can provide various benefits in multiple applications,[15] including ecological restoration, sensing, imaging, drug delivery and catalysis.[16] Furthermore, bimetallic nanoparticles are employed in environmental remedial measures for degrading unwanted pollutants in the water and soil environments, demonstrating their potential to solve complex environmental challenges.[17]

In the conventional method, harsh chemicals and high temperatures are used for the synthesis of bimetallic and other

[a]*Department of Chemistry, St. Berchmans College (Autonomous), Mahatma Gandhi University, Kottayam, India. E-mail: sajinijebin@sbcollege.ac.in*

[b]*Department of Botany, St. Berchmans College (Autonomous), Mahatma Gandhi University, Kottayam, India*

[c]*Department of Microbiology & Biochemistry, St. Berchmans College (Autonomous), Mahatma Gandhi University, Kottayam, India*

nanomaterials, raising concern about their environmental impacts and potential health hazards.[18] Because of the increased concerns about the potential effects of conventional chemical processes on the environment and human health, there has been a greater focus on sustainable and greener approaches for nanoparticle synthesis.[8] Microwave radiation, for example, is an appealing technique that offers fine control over nanoparticle characteristics, including faster heating, shorter reaction times and better yields.[19] Additionally, it is well known that plant extract can be used as a reducing and stabilising agent that provides a green alternative to conventional chemical methods, contributing to sustainable nanoparticle synthesis.[20]

The bimetallic nanoparticles of silver and zinc oxide are well known for their antimicrobial activity and their potential in photocatalytic applications.[21] However, many of these bimetallic nanoparticles rely on chemical synthesis methods[22] that can be environmentally hazardous and may result in nanoparticles with less desirable biocompatibility. Reports are also available for the biogenic synthesis of these bimetallic nanoparticles for varying applications.[17,21,23] The present investigation focused on the green and sustainable synthesis of bimetallic silver and zinc oxide nanoparticles (Ag/ZnO-NPs) using plant extract (*Hylocereus costaricensis*) and investigated the antimicrobial potential of the green synthesised Ag/ZnO nanoparticles. Compared to other green synthesis strategies, here silver and zinc oxide nanoparticles were synthesized separately and then directly mixed to form bimetallic nanoparticles (Ag/ZnO-NPs).

The *Hylocereus costaricensis* (HC) stem is included throughout nanoparticle synthesis, emphasising the study of sustainable methodology.[24,25] HC, often called dragon fruit, is a tropical cactus species well known for its vivid appearance and medicinal properties.[26] The stem extract of HC comprises many phytochemicals such as flavonoids, polyphenols and antioxidants[27,28] that serve as a vital source for synthesising nanoparticles, including bimetallic nanoparticles, using green synthesis methods.[29,30]

The synthesised nanoparticles were thoroughly characterized using field-emission scanning electron microscopy (FE-SEM), energy-dispersive X-ray spectroscopy (EDX), Fourier-transform infrared spectroscopy (FT-IR), dynamic light scattering (DLS), zeta potential and X-ray diffraction (XRD). Additionally, the antibacterial efficacy of Ag/ZnO-NPs against two major human pathogens *Escherichia coli* and *Staphylococcus aureus* was tested using the conventional agar well diffusion method.[31,32] All the characterisation techniques confirmed the successful synthesis of bimetallic nanoparticles with a unique morphology and enhanced properties. Antibacterial studies revealed that Ag/ZnO-NPs demonstrated superior antibacterial activity compared to individual Ag-HC and ZnO-HC nanoparticles, highlighting their potential as effective antibacterial agents from renewable sources.

The present methodology offers a favourable avenue for addressing complex challenges in antibacterial studies. With this method, we emphasise contributing to the sustainable development and environment-friendly synthesis of antibacterial agents, thereby advancing biomedical research and healthcare. The study intends to contribute significantly to the developing field of bimetallic nanoparticles and their possible uses in biomedicine and other fields by thoroughly characterising and assessing their antibacterial activity. It also focuses on the significance of sustainable synthetic methods in nanoparticle research.

2. Experimental

2.1 Materials

$AgNO_3$ and $ZnSO_4$ have been purchased from Merck in India. All the chemicals used were of analytical grade and used exactly as purchased, without any additional purification processes.

2.2 Methodology

2.2.1 Collection, purification, and extraction of HC stem extract. In October 2023, specimens of *Hylocereus costaricensis* were obtained from the Eduthumparambu region in Ponkunnam, Kerala, India. The fresh stems of *Hylocereus costaricensis* were explicitly selected and taxonomically identified. Then, it was thoroughly washed with distilled water to remove all the debris and dust and cut into little pieces. The sample was oven-dried and powered using a motor and pestle. The plant extract was prepared as per standard protocols.[8–10] In brief, 100 mL of distilled water was added to a round-bottom flask, fitted with a condenser, containing 25 grams of the dried stem sample and the mixture was boiled for 30 minutes. Upon cooling, if any solid residues were there, they were filtered out using Whatman filter paper to obtain the HC stem extract, which was then refrigerated for further use.

2.2.2 Synthesis of Ag-HC and ZnO-HC. A 2 mM solution of $AgNO_3$ (120 mL) was prepared in a beaker to synthesise silver nanoparticles. 30 mL of HC stem extract was added to the above mixture and stirred well. The resulting solution was then exposed to microwave radiation using a Sharp R219T (W) model microwave oven that operates at a frequency of 2450 MHz and power of 800 W. The radiation was conducted for about six minutes, and a UV-visible spectrophotometer was used to observe the growth of silver nanoparticles (Ag-HC). The samples were taken at one-minute intervals of up to six minutes to examine the development of Ag-HC formation (Scheme 1).

Similarly, to synthesise zinc oxide nanoparticles (ZnO-HC), a 2 mM solution of zinc sulphate (120 mL) was made in a beaker. After this, 30 mL of the HC extract was added to the above solution and mixed well. The resulting solution was then exposed to microwave radiation under working conditions as in Ag-HC synthesis. During the radiation process, the formation of zinc oxide nanoparticles was observed using a UV-visible spectrophotometer. The samples were taken every minute for a maximum of six minutes to monitor the development of ZnO-HC formation (Scheme 1).

2.2.3 Synthesis of bimetallic Ag/ZnO-NPs. A simple method of direct mixing of two metal nanoparticle solutions produced the bimetallic silver and zinc oxide nanoparticles (Scheme 1). For this, in a conical flask, precisely 30 mL of Ag-HC and 30 mL

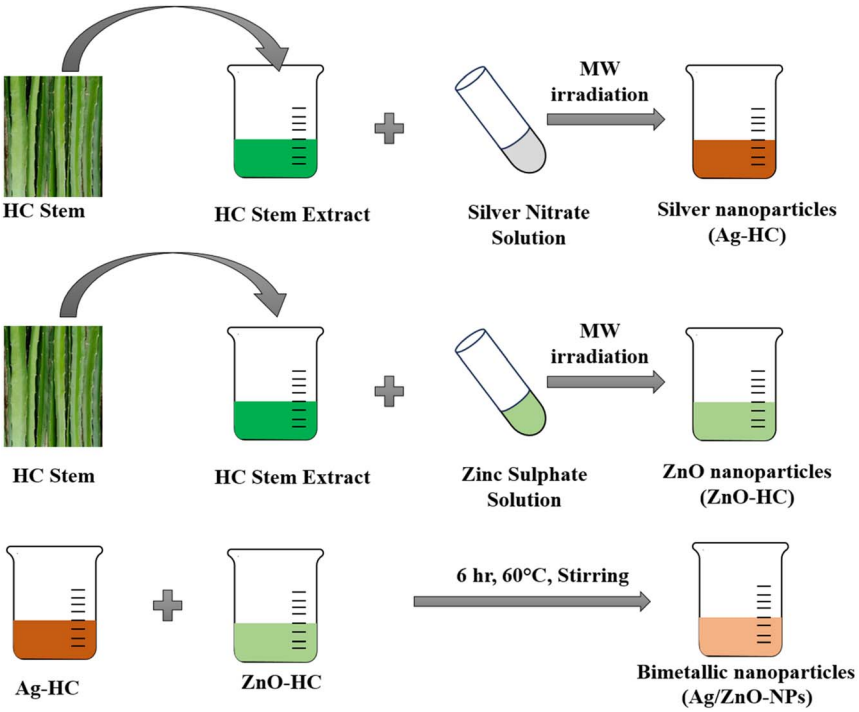

Scheme 1 Schematic representation of the formation of Ag-HC, ZnO-HC and Ag/ZnO-NPs.

of ZnO-HC were thoroughly mixed and stirred for about six hours by maintaining the temperature at 60 °C. The resulting bimetallic nanoparticle solution of Ag/ZnO-NPs was subsequently refrigerated and stored for further analysis and use.

2.2.4 Antibacterial studies. The antibacterial activity of the synthesised nanoparticles was investigated using the traditional agar well diffusion technique against prevalent bacteria that cause diseases in humans, such as *Staphylococcus aureus* and *Escherichia coli*.[8] For this, a sterile cork borer was used to create wells on each plate after the cultures of bacterial strains were swabbed into nutritious agar sheets. Afterwards, 100 μL of nanoparticle samples (Ag-HC, ZnO-HC, and Ag/ZnO-NPs) were filled into the corresponding wells, and six replicates were prepared for each sample. Ciprofloxacin, a standard commercial antibiotic disc, was used as the positive control (PC), and plant extract was used as the negative control (NC). These plates were then kept for an incubation period of 24 hours at a temperature of 37 °C. Each of the well's zones of inhibition was determined after incubation. Gram-negative *Escherichia coli*, responsible for digestive disorders and infections of the urinary system,[9] and Gram-positive *Staphylococcus aureus*, which results in multiple illnesses, including skin and connective tissue, were the selected species for the antimicrobial research.[8]

2.2.5 Characterization studies adopted. A multitude of analytical methods were utilised to comprehensively study the shape, structure, and physical and chemical aspects of developed Ag-HC, ZnO-HC and bimetallic Ag/ZnO-NPs. These approaches offered a distinct viewpoint on the various features of nanoparticles. Using a PerkinElmer Spectrum two FT-IR spectrometer, Fourier transform infrared spectroscopy (FT-IR) was used to evaluate the underlying functional groups of the nanomaterials and any chemical reactions that occurred among the nanoparticles and the stabilising molecules.[33] Also, by making use of a Shimadzu UV-2450 spectrophotometer, UV-visible spectrophotometry analysis was performed to look into the spectral characteristics of the nanoparticles, namely their absorption spectra, which facilitated understanding of their electrical structure and stable nature.[34] By employing the Rigaku miniflex 600 XRD apparatus, X-ray diffraction (XRD) analysis was used to assess the crystalline structure and phase purity of nanoparticles. This method assisted in the identification of crystallographic phases and the estimation of crystallite size.[35] Superior resolution visualisation of the dimensions and surface appearance of the nanoparticles was made possible using field emission scanning electron microscopy (FE-SEM), which specified data regarding the dimensions, form, and aggregation state of the particles.[36] Here, MAIA3XMH FE-SEM with energy dispersive technology were used. Through conducting quantitative assessments of elemental dispersion and composition, the chemical composition of the nanoparticles was determined by using FE-SEM in conjunction with energy dispersive spectroscopy (EDS), hence verifying the existence of iron, silver, and oxygen.

For the EDX analysis, the synthesised nanoparticles were first dried in a vacuum oven at 60 °C for 12 hours. A small amount of the dried sample was then placed on carbon tape attached to an aluminium stub. To enhance conductivity and improve imaging quality, the sample was coated with a thin layer of gold using a sputter coater for 60 seconds at 20 mA. The gold-coated sample was analysed using a field-emission scanning electron microscope (FE-SEM) equipped with an energy-

dispersive X-ray (EDX) detector under high vacuum conditions with an accelerating voltage of 20 kV. EDX spectra were collected from multiple sample regions, with the data acquisition set to 60 seconds per region.

Determining the nanoparticles' stable nature and colloidal properties in solution requires thorough knowledge of their external charge on the surface as well as their distribution of size, which can be achieved through dynamic light scattering (DLS) and zeta potential examinations by employing a nanoparticle analyzer-Horiba SZ-100.[37] Ag-HC, ZnO-HC, and bimetallic Ag/ZnO-NPs were thoroughly investigated for future uses in biological, medicine, sensing, and catalysis processes owing to the wide variety of employed characterization approaches.

3. Results and discussion

3.1 UV-visible spectrophotometric analysis

The synthesized nanoparticles' optical characteristics and the development of their formation during the process can be better understood by analysing them using a UV-visible spectrophotometer. There may be a progressive rise in absorbance readings from one to six minutes into the synthesis, indicating the ongoing development and formation of silver nanoparticles. Regarding Ag-HC (Fig. 1), a broad absorption peak in the 400–450 nm range and a peak in the 250–350 nm range were observed in the spectrum, revealing the formation of metallic silver and silver oxide nanoparticles, respectively.[38] These peaks correspond to the surface plasmon resonance (SPR) absorption peaks of silver nanoparticles.[39] In the UV-visible spectrum, ZnO-HC nanoparticles exhibit an evident absorbance peak at 291 nm, associated with the electronic transitions related to the zinc oxide band structure (Fig. 2).[40] The valence band to conduction band transitions or intra-band transitions within the zinc oxide nanoparticles could be the source of this peak. As the ZnO-HC nanoparticles grow and develop throughout the synthesis, the absorbance values in this peak may sometimes rise.

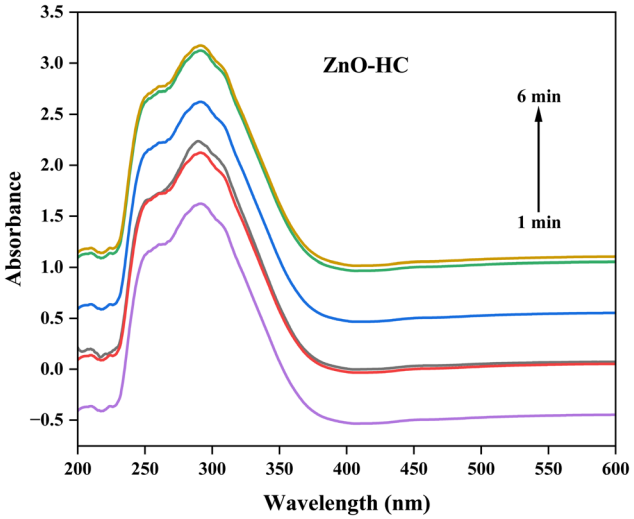

Fig. 2 UV-visible spectrum of ZnO-HC.

Compared to the separate Ag-HC and ZnO-HC spectra, the bimetallic Ag/ZnO-NPs exhibited a slight shift in the absorbance peak of the UV-visible spectrum (Fig. 3).[41,42] This shift could mean that interactions exist among the zinc oxide and silver nanoparticles that constitute the bimetallic system and are responsible for the variations in the optical characteristics of these nanoparticles. Due to the existence of both nanoparticles in the bimetallic system, the absorbance values at distinctive peaks of zinc oxide and silver could deviate somewhat from those of their solo counterparts.[20] The SPR band of silver nanoparticles is typically observed as a distinct peak in the UV-visible spectra due to the collective oscillation of electrons at the nanoparticle surface. In the case of Ag/ZnO-NPs, this SPR band may be suppressed or shifted due to the interaction between silver and zinc oxide, which could affect the electronic environment of the silver nanoparticles.

The kinetic and optical activity of the nanoparticles can be obtained from the UV-visible spectrophotometric data,

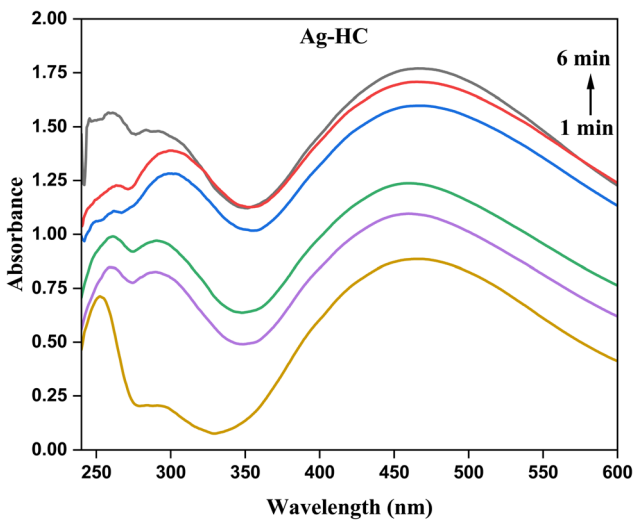

Fig. 1 UV-visible spectrum of Ag-HC.

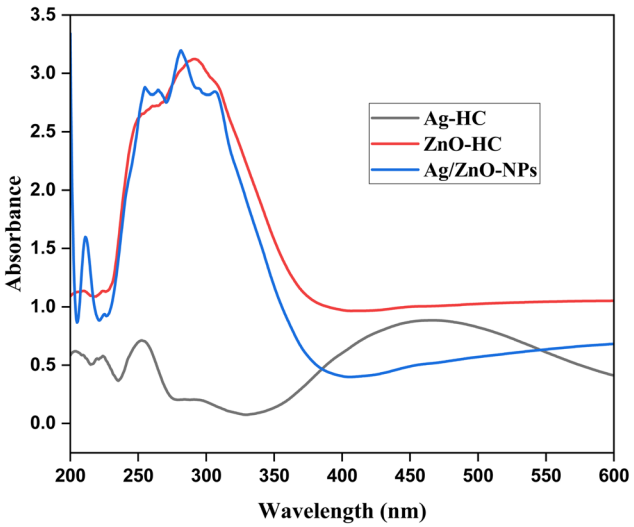

Fig. 3 UV-visible spectra of Ag-HC, ZnO-HC and Ag/ZnO-NPs.

indicating the production and development of Ag-HC, ZnO-HC and bimetallic Ag/ZnO-NPs with time. The kinetic results obtained from Fig. 1 revealed the synthesis progression of silver nanoparticles using HC stem extract, monitored *via* UV-visible absorption spectra at 1 to 6-minute intervals. Initially, a weak and broad absorption peak at 1 minute indicates the early formation of nanoparticles. As the reaction progresses to 2 and 3 minutes, the peak intensity increases and narrows, reflecting the growth and accumulation of nanoparticles. The absorption peak stabilises by 4 to 6 minutes, indicating that the synthesis process is nearing completion and the nanoparticles have achieved a consistent size distribution. The changes in peak intensity and shape provide insight into the rate of nanoparticle formation and growth dynamics.

The direct band gaps obtained from Tauc plots of Ag-HC, ZnO-HC, and Ag/ZnO-NPs are 3.24 eV, 3.33 eV, and 2.90 eV, respectively as depicted in Fig. 4. The direct band gap of 3.24 eV for Ag-HC indicates notable quantum confinement effects, highlighting the nanoparticles' reduced size and altered electronic properties compared to bulk silver.[43] This band gap suggests that Ag-HC nanoparticles can effectively absorb high-energy photons, making them suitable for UV-active applications such as photocatalysis and optical sensors.[44] The green synthesis method ensures environmental sustainability and potential biocompatibility, enhancing their appeal for various biomedical and environmental applications. ZnO-HC exhibits a direct band gap of 3.33 eV, slightly lower than the typical band gap of bulk ZnO (3.37 eV).[45,46] This minor reduction may result from interactions with organic molecules from the plant extract, subtly modifying the nanoparticles' electronic structure. The band gap value indicates strong UV light absorption capabilities, making ZnO-HC nanoparticles ideal for applications in UV photodetectors and photocatalytic degradation of pollutants, and as effective antibacterial agents due to their potential to generate reactive oxygen species.[47] The lower band gap energy of 2.90 eV for Ag/ZnO-NPs compared to that of Ag-HC and ZnO-HC suggests enhanced light absorption capabilities, particularly in the visible range.[22,48] This reduction in the band gap implies improved electronic and optical properties, making these nanoparticles potentially more effective in applications like photocatalysis and sensing.[49]

A proposed mechanism involved in forming Ag-HC, ZnO-HC and Ag/ZnO-NPs is depicted in Scheme 2 and described as follows. The components of the HC stem extract elaborately coordinate a sequence of processes that gave rise to the mechanism leading to the synthesis of Ag-HC. The interaction between the silver ions (Ag) derived from a silver salt precursor and phytochemicals such as flavonoids and polyphenols present in the HC stem extract initiates the formation of silver nanoparticles. These phytochemicals act as potent reducing agents by accelerating the transfer of electrons to silver ions (Ag^{+}) and causing their reduction to silver atoms (Ag^{0}).[31,50] Several tiny clusters of nanoparticles are then generated due to the aggregation and nucleation of freshly generated silver atoms.[51] Because of an ongoing supply of reducing agents by the stem extract, the aggregation and reduction of nanoparticles continue. As the reaction progresses, some silver nanoparticles

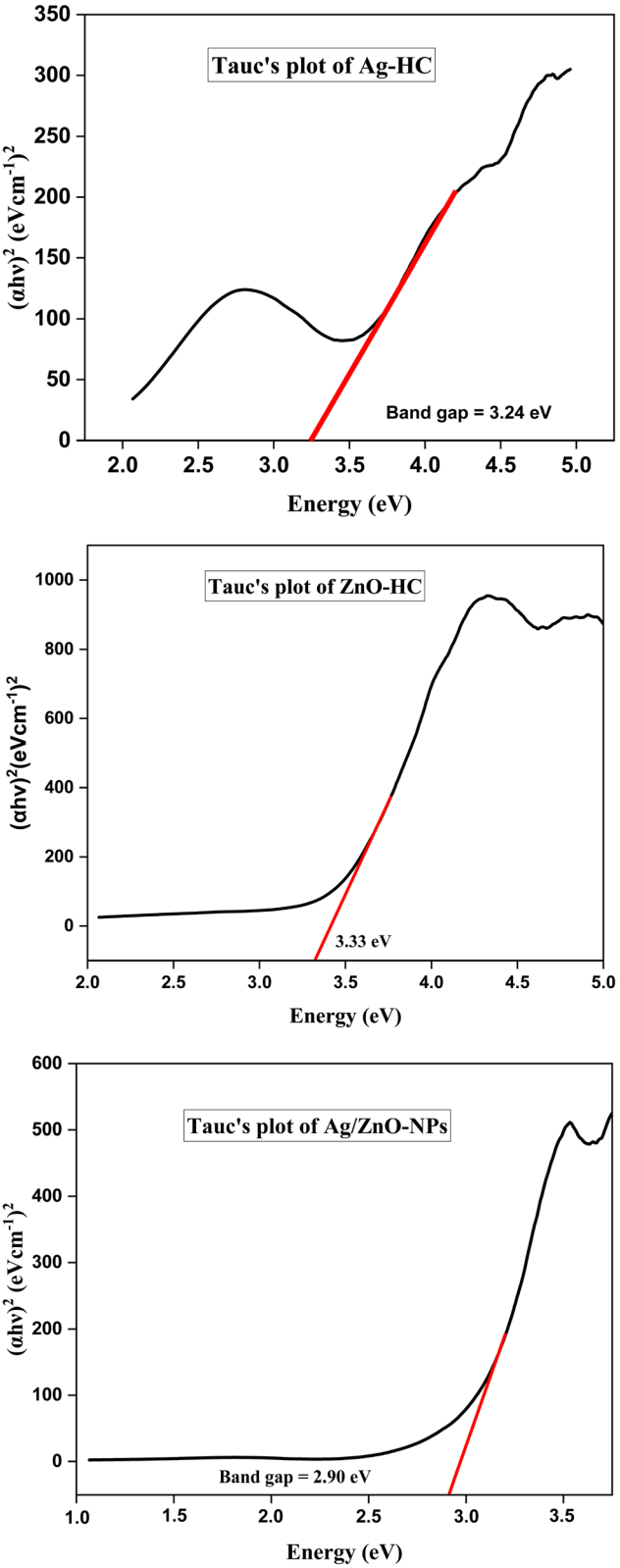

Fig. 4 Tauc plots of Ag-HC, ZnO-HC and Ag/ZnO-NPs.

may undergo partial oxidation in the presence of oxygen or other oxidising species in the reaction mixture. This leads to silver oxide (Ag_2O) forming on the surface of the nanoparticles.[52] Simultaneously, phytochemicals included in the

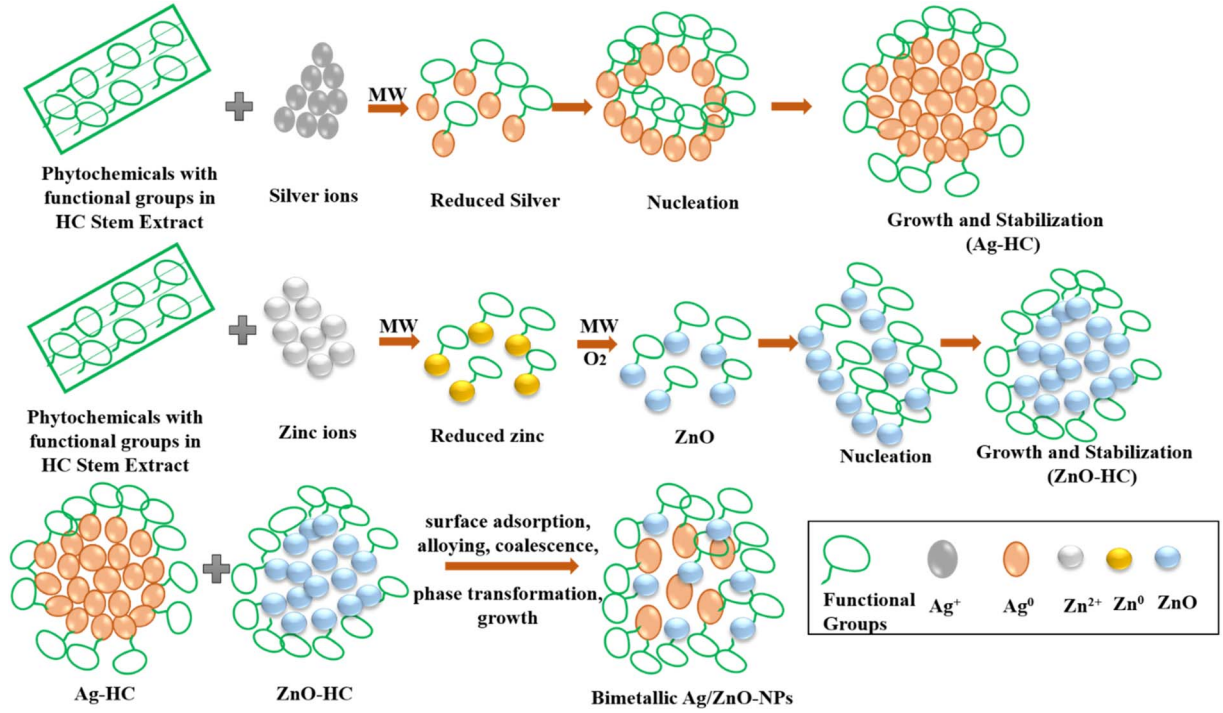

Scheme 2 Plausible mechanism involved in the formation of Ag-HC, ZnO-HC and Ag/ZnO-NPs.

extract show a preference for the surfaces of the nanoparticles at which they absorb and function as reducing and stabilising agents.[53,54] This dual purpose keeps the formed Ag-HC nanoparticles stabilised and dispersed by avoiding unwanted agglomeration and maintaining the well-defined structure of particles. Ag-HC is synthesised *via* a complex interaction between phytochemicals and silver ions, resulting in nanoparticles having beneficial features for various uses.

As ZnO-HC synthesis occurs, the phytochemicals found in the HC stem extract first reduce the zinc ions (Zn^{2+}) present in the precursor solution.[47] The phytochemicals consist of flavonoids, polyphenols, and other organic substances that act as reducing agents by transferring electrons to zinc ions. Zinc oxide (ZnO) nuclei were formed due to the reduction, and the nuclei eventually grew due to the aggregation and nucleation processes. The hydroxyl group (OH^-) in the HC extract facilitates nucleation and stabilisation and hence aids in generating zinc oxide nanoparticles.[55] Zinc ions then react with these hydroxyl groups and get hydrolysed to produce zinc hydroxide [$Zn(OH)_2$], which subsequently proceeds through dehydration and condensation and leads to the generation of ZnO nuclei.[56] Phytochemicals in the HC extract attach to the surface of the developing ZnO particles, thus functioning as capping agents to avoid agglomeration and stabilise the nanoparticle structure.

Various crucial steps are involved in generating bimetallic Ag/ZnO-NPs formed by the direct combination of Ag-HC and ZnO-HC solutions, which were synthesised in advance.[21,23] First, phytochemicals found in the HC stem extract are used to individually reduce the corresponding metal ions of silver and zinc oxide to form stabilized silver and zinc oxide nanoparticles. Electrostatic interaction among the nanoparticles promotes their aggregation and deposition of one metal onto the surfaces of others due to diffusion on combining these solutions. Organic ligands or biomolecules in the plant extract also act as mediators in the nanoparticle interactions, promoting stabilisation. The combination process allows close interaction and connection between Ag and ZnO nanoparticles, ultimately generating bimetallic Ag/ZnO-NPs with unique characteristics and synergistic effects.

3.2 FT-IR analysis

The Fourier transform infrared spectroscopy (FT-IR) spectra of HC stem extract, Ag-HC, ZnO-HC, and bimetallic Ag/ZnO

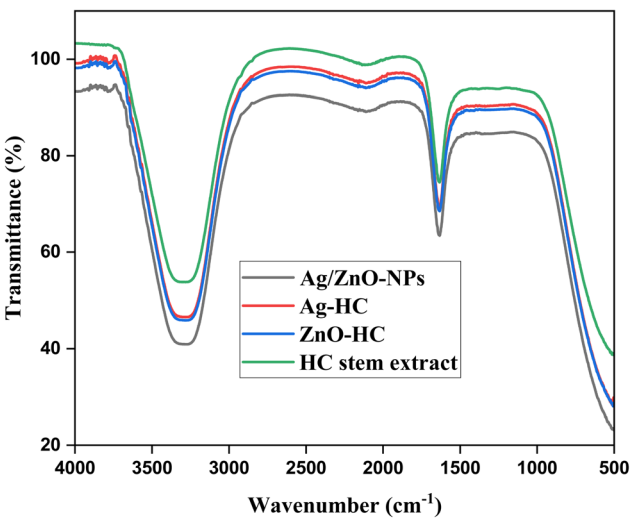

Fig. 5 FT-IR spectra of HC stem extract, Ag-HC, ZnO-HC and Ag/ZnO-NPs.

nanoparticles (Ag/ZnO-NPs) revealed important functional groups and possible chemical interactions present in the production method (Fig. 5). The individual peaks characteristic of the different functional groups in the extract can be seen in the FT-IR spectra of the HC stem extract. The hydroxyl (–OH) groups' stretching vibrations commonly linked to the phenols, alcohols and carbohydrates present in the extract are shown by a prominent peak in the range of 3200–3300 cm^{-1}.[57] Furthermore, the peak at 1630 cm^{-1} is consistent with the carbonyl (C=O) groups' stretching vibration, suggesting the existence of carbonyl compounds such as aldehydes and ketones.[58] Comparable peaks attributed to the –OH groups and carbonyl (C=O) groups were visible in the FT-IR spectra of the Ag-HC produced utilising HC stem extract, thereby suggesting that the biomolecules of the extract have been absorbed upon the Ag-HC nanoparticle surface. The shifts or deviation in the intensities of the peaks when compared to those of the HC stem extract indicated the association between silver nanoparticles and biomolecules, suggesting that the biomolecules could function as stabilising or capping agents at the time of nanoparticle formation. Similar to the HC stem extract spectra, the FT-IR spectra of ZnO-HC formed using the extract showed peaks corresponding to –OH groups and carbonyl (C=O) groups, indicating that the biomolecules have adhered to the ZnO-HC surface, which may have an impact on stabilising and altering the surface of nanoparticles. Lastly, the peaks associated with carbonyl groups and –OH groups are visible in the FT-IR spectrum of bimetallic Ag/ZnO-NPs produced utilising HC stem extract; these peaks are like those seen in the spectra of both the HC stem extract and the isolated nanoparticles with some changes in the peak intensities. This suggested the adhering of biomolecules onto the surfaces of silver and zinc oxide nanoparticles, which could impact the stabilisation and connection of the nanoparticles within the bimetallic system. These findings highlight the unique interactions and structural modifications in bimetallic Ag/ZnO nanoparticles. By clarifying the molecular mechanisms that contribute to the creation of nanoparticles and their surface alteration, the FT-IR spectra provide significant knowledge about the functional groups found within the HC stem extract and how they react with the produced nanoparticles.

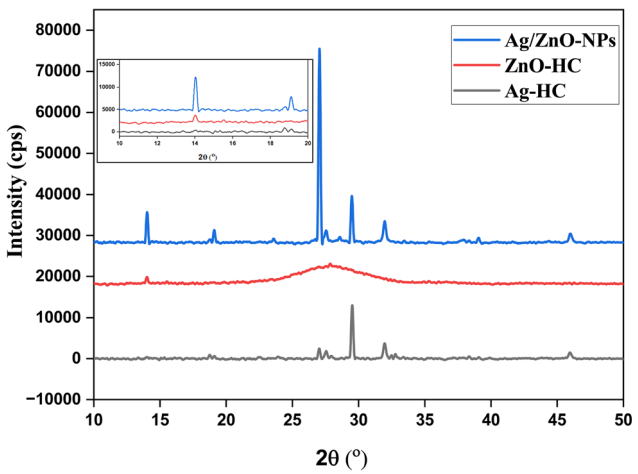

Fig. 6 XRD patterns of Ag-HC, ZnO-HC and Ag/ZnO-NPs. The inset shows the magnified XRD patterns of mono and bimetallic nanoparticles.

3.3 XRD analysis

The individual patterns characteristic of the crystalline structures of nanoparticles are unveiled by the X-ray diffraction (XRD) analysis of Ag-HC, ZnO-HC and Ag/ZnO-NPs (Fig. 6). In Ag-HC, the 2θ angle corresponding to 32.08, 45.9, 38.32, 27.6 and 18.7 are equivalent to the (111), (200), (220), (311), and (222) face-centred cubic planes of silver, respectively.[59] The zinc oxide hexagonal wurtzite planes (002) and (101) are represented by the two notable ZnO-HC peaks, which appeared at 27.8 and 14.1, respectively.[20] The observed amorphous phase in the XRD results for ZnO-HC could be attributed to several factors. The small size of the ZnO-HC nanoparticles might lead to broad and poorly defined peaks, giving an overall amorphous appearance.[60] Also, the synthesis conditions, such as temperature and reaction time, could influence the degree of crystallisation. The XRD spectrum showed peaks associated with silver and zinc oxide during bimetallic Ag/ZnO-NP production, verifying that both phases exist in bimetallic nanoparticles.[20,42] Bimetallic Ag/

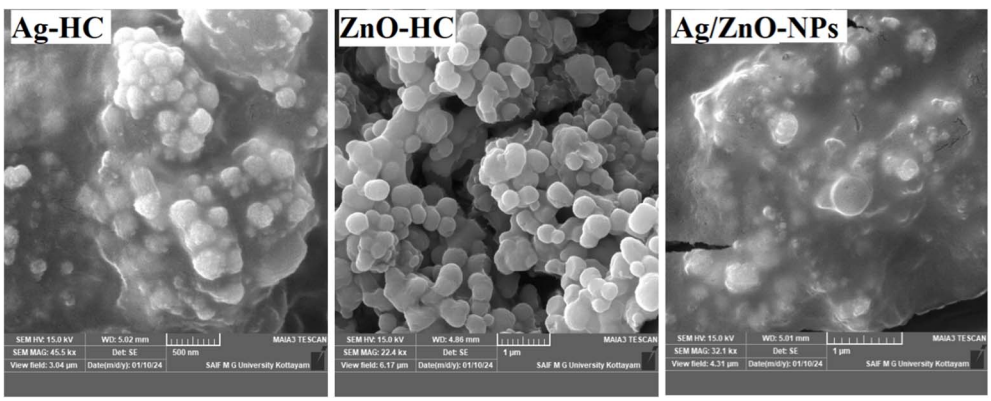

Fig. 7 FE-SEM images of Ag-HC, ZnO-HC and Ag/ZnO-NPs.

ZnO-NPs with a heterostructure crystalline framework were quickly created, as evidenced by extra peaks, variations in the peak intensities and alterations in the position of peaks compared to the Ag-HC and ZnO-HC spectra.[61] These changes may indicate alloying or potential associations that exist between two of the materials.

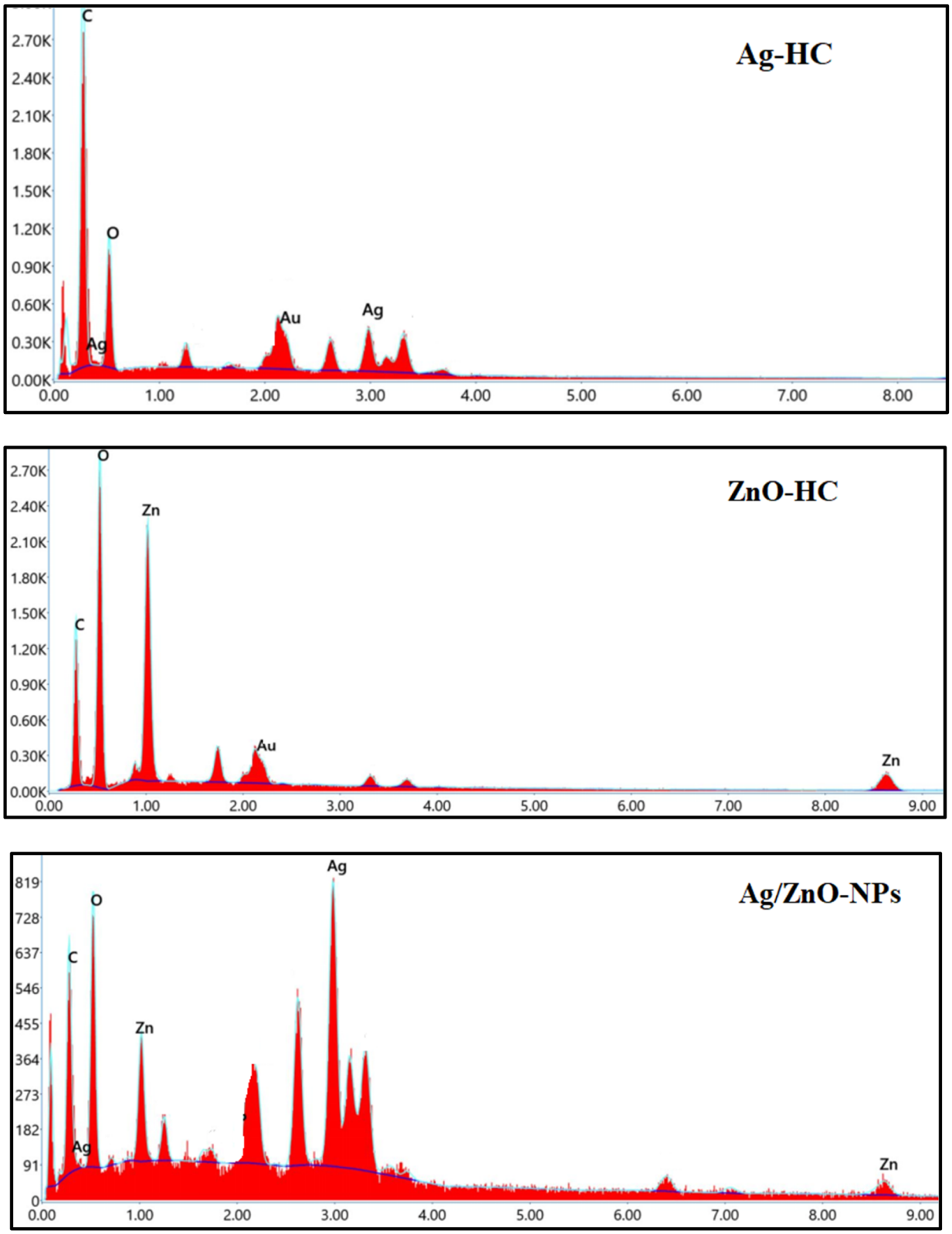

Fig. 8 EDX spectra of Ag-HC, ZnO-HC and Ag/ZnO-NPs.

3.4 FE-SEM analysis

The FE-SEM analysis showed unique ZnO-HC, Ag-HC and Ag/ZnO-NP morphologies (Fig. 7). Ag-HC presents a partly spherical form with imperfections on the surface, suggesting the nucleation and development process characteristic of the silver nanoparticles from the plant extract.[62] On the other hand, ZnO-HC exhibited a fine surface and an impeccable spherical form of the zinc oxide nanoparticles generated using comparable techniques.[55] Ag/ZnO-NPs, in this instance, exhibited both forms, some displaying perfectly spherical forms like that of ZnO-HC and others displaying partly spherical forms like Ag-HC.[20] This evidence indicated that the zinc oxide and silver nanoparticles are part of a bimetallic system, partially preserving their structures.

3.5 EDX analysis

The elements that constitute the nanoparticles formed were revealed by the EDX analysis of Ag-HC (Fig. 8). The significant observation of the peaks characteristic of silver in the Ag-HC spectra can verify the existence of silver nanoparticles.[63] Also, the peaks characteristic of zinc and oxygen are visible in the ZnO-HC spectra, confirming the existence of zinc oxide nanoparticles.[55] However, a peak characteristic of both silver and zinc can be identified in the Ag/ZnO-NP spectrum, indicating the existence of both nanoparticles in the bimetallic system.[41] Furthermore, an oxygen peak is substantial evidence confirming the generation of zinc oxide nanoparticles. Therefore, the EDX analysis technique agrees with the bimetallic nature of Ag/ZnO-NPs and explains its elemental composition, also validating the efficacy of the synthetic approach adopted in the formation of Ag-HC, ZnO-HC and Ag/ZnO-NPs.[42]

3.6 DLS analysis

The data concerning nanoparticle hydrodynamic diameter were obtained in the solution using the DLS technique, indicating the particle size distribution (Fig. 9).[64] The observed hydrodynamic diameter of 141.7 nm for Ag-HC indicated the existence of silver nanoparticles in a considerably narrower size distribution.[65] On the other hand, ZnO-HC showed a significantly reduced hydrodynamic diameter of 0.5 nm but displayed a broader size distribution of zinc oxide nanoparticles compared to Ag-HC.[55] Significantly, the hydrodynamic diameter of Ag/ZnO-NPs increased to about 281.7 nm, slightly larger than that of Ag-HC and maintained a narrow distribution similar to that of Ag-HC. These differences in size and distribution indicate the bimetallic nanoparticles' unique formation and stability characteristics. The observed size enhancement indicated the effective production of bimetallic Ag/ZnO-NPs. It could be the possible associations among the two types of nanoparticles that cause the nanoparticles to coalesce or aggregate and hence produce large clusters.

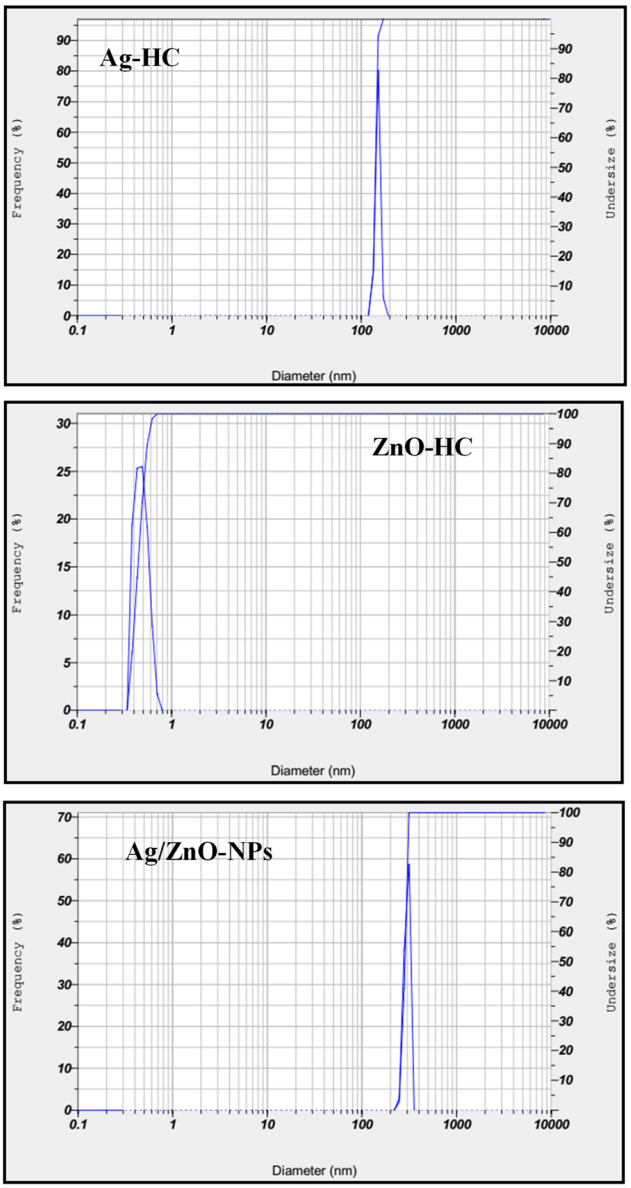

Fig. 9 DLS graphs of Ag-HC, ZnO-HC and Ag/ZnO-NPs.

3.7 Zeta potential analysis

The zeta potential results gave information about how stable the nanoparticles were in the solution; higher positive or negative values correspond to more stable nanoparticles because of the greater electrostatic repulsion that exists among the particles (Fig. 10).[32] The zeta potential analysis revealed that the zeta potentials of Ag-HC, ZnO-HC, and bimetallic Ag/ZnO-NPs were −15.7 mV, −10.1 mV, and −11.7 mV, respectively. This indicated that the bimetallic Ag/ZnO nanoparticles are less stable than the Ag-HC nanoparticles but exhibit excellent stability compared to the ZnO-HC nanoparticles. The zeta potential value of −11.7 mV for Ag/ZnO-NPs, being closer to −10.1 mV of ZnO-HC, suggests that the ZnO component influences the stability characteristics of the bimetallic nanoparticles more.[55]

3.8 Antibacterial studies

In contrast to the negative control, HC-stem extract, antibacterial activity findings showed how efficient Ag-HC and ZnO-NPs

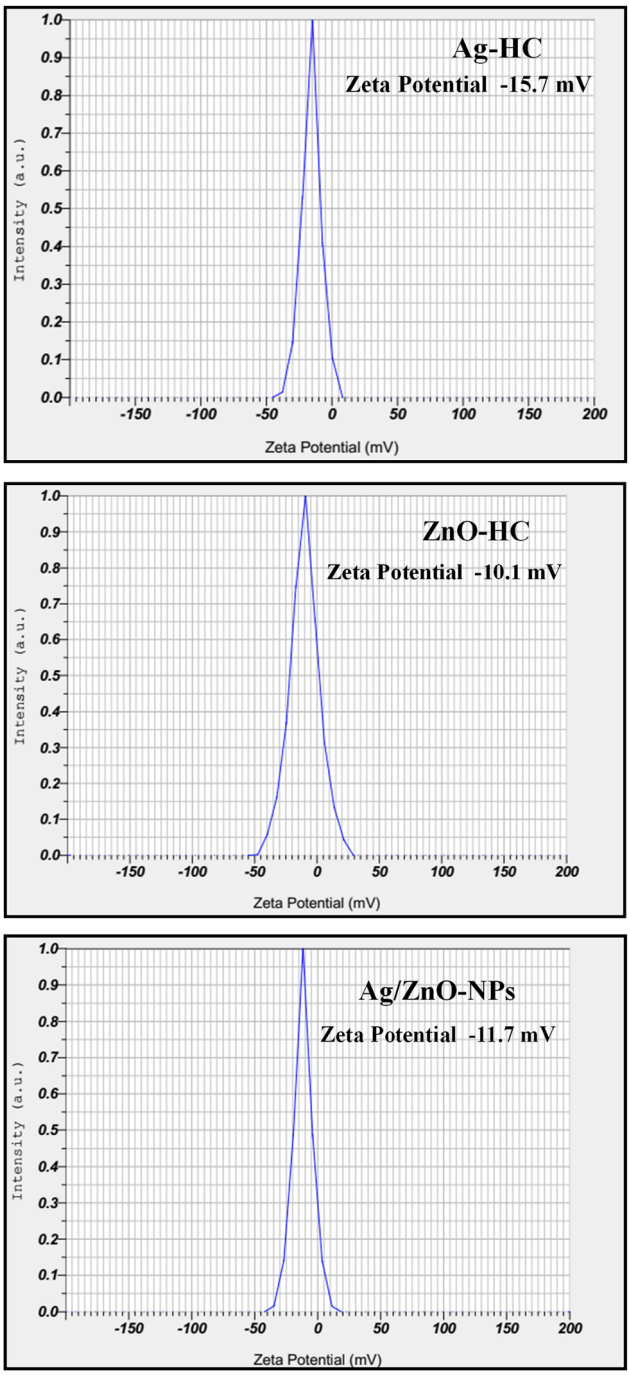

Fig. 10 Zeta potential graphs of Ag-HC, ZnO-HC and Ag/ZnO-NPs.

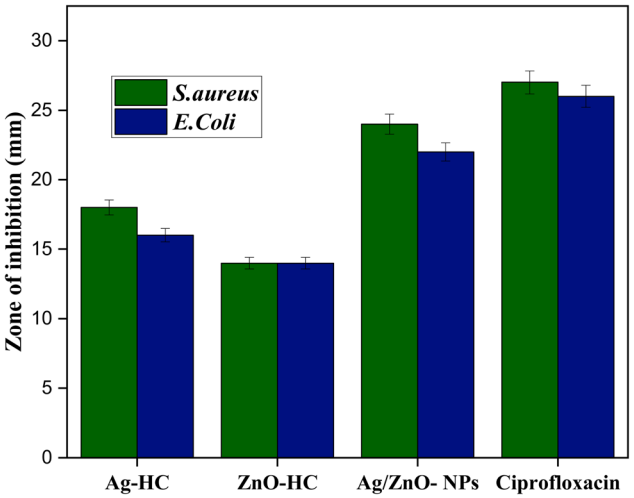

Fig. 11 Zone of inhibition exhibited by *S. aureus* and *E. coli* bacterial strains.

are towards *S. aureus* and *E. coli*, the two most prevalent pathogenic bacteria (Fig. 11).[66] The stem extract showed no antibacterial activity towards the two bacterial strains. Ag-HC exhibited significant antibacterial properties with inhibition zones of 18 mm against *E. coli* and 16 mm to oppose *S. aureus*. ZnO-HC has a modest antibacterial activity against the two bacterial strains, with smaller inhibition zones of 14 mm.[67] Among these specimens, Ag/ZnO-NPs exhibit the best antibacterial activity, nearer to that of ciprofloxacin, with inhibition zones measuring 24 mm against *S. aureus* and 22 mm against *E. coli*. Ag/ZnO-NPs' increased antibacterial efficiency indicated the beneficial effects of mixing silver and zinc oxide nanoparticles, which makes them an appealing option for fighting diseases.[23] Based on the study's outcomes, bimetallic nanoparticles may have significant antibacterial activities, which could aid in the creation of antimicrobial substances which perform well for a range of potential biological uses. The reliability of the experimental approach can be confirmed since the positive control, ciprofloxacin, constantly showed antimicrobial properties towards *E. coli* and *S. aureus*.

Several elements contribute to the antibacterial properties of Ag-HC, ZnO-HC, and Ag/ZnO-HC. In the context of Ag-HC, silver nanoparticles (AgNPs) are recognised for their antibacterial qualities, mainly caused by the release of silver ions (Ag^{+}) that damage the cell membranes of bacteria, obstruct biological functions, and cause oxidative stress, eventually destroying microbial cells.[68] Zinc oxide nanoparticles (ZnO-NPs) produce reactive oxygen species (ROS) on their surface when exposed to light or oxygen; due to this reason, ZnO-HC possesses significant antimicrobial properties.[55] ROS can destroy microbial cells by destroying bacteria's proteins, DNA, and cell wall membranes. Silver and zinc oxide nanoparticles combine effectively to increase the antibacterial properties of the bimetallic Ag/ZnO-NPs (Scheme 3).[23] Both Ag-HC and ZnO-HC can function separately or in combination, focusing on distinct microbial elements and amplifying both of their antibacterial properties.[69] Bimetallic nanoparticles' distinctive features, particularly their increased surface area and modified surface chemistry, may also improve their ability to attach to bacterial cell walls, resulting in greater antibacterial efficiency. Combining silver and zinc oxide nanoparticles mediates the antibacterial mechanism of Ag-HC, ZnO-HC, and Ag/ZnO NPs. The effect involves destroying bacterial cells by damaging membranes, producing reactive oxygen species (ROS), and disrupting cellular activities.[70,71]

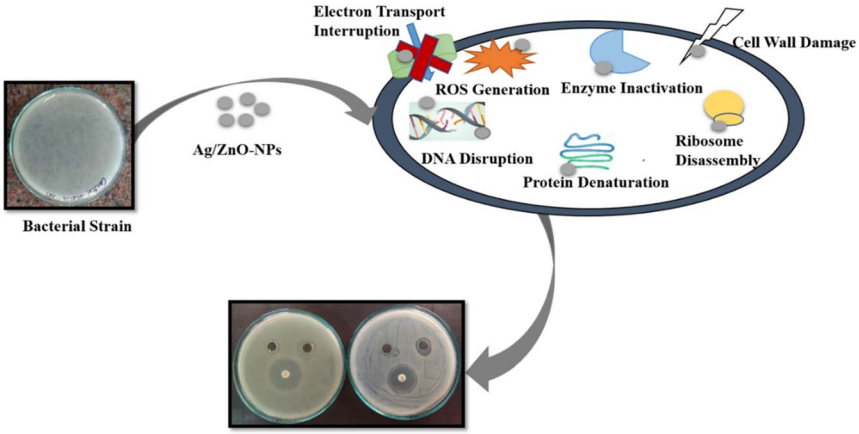

Scheme 3 Schematic representation of the antibacterial activity of Ag/ZnO-NPs.

4. Conclusion

The present research study summarises the possibility of using environmentally friendly and sustainable methods in bimetallic nanoparticle formation. Specifically, bimetallic silver and zinc oxide nanoparticles (Ag/ZnO-NPs) were synthesised using the stem extract of *Hylocereus costaricensis* (HC) and microwave radiation. We were able to fully characterise the produced nanoparticles and ascertain their shape, structural and functional characteristics by utilising several analytical methods, which included UV-visible spectrophotometry, energy-dispersive X-ray spectroscopy, dynamic light scattering, Fourier-transform infrared spectroscopy, and field-emission scanning electron microscopy. FT-IR analysis confirmed the presence of functional groups from the stem extract, indicating successful capping and stabilisation of the nanoparticles. FE-SEM images revealed that the Ag/ZnO-NPs possessed a unique cluster-like spherical morphology. XRD analysis showed distinct diffraction peaks corresponding to silver and zinc oxide, with significant changes in peak intensities, confirming the formation of bimetallic nanoparticles. In the antibacterial investigation, Ag/ZnO-NPs demonstrated substantial potential activity against two human pathogenic bacteria, *Staphylococcus aureus* and *Escherichia coli*; this suggests that they could be utilised as environmentally benign antimicrobial agents. Furthermore, the combined silver and zinc oxide nanoparticle-mediated effects, such as membrane rupture, disruption of cellular activities, and reactive oxygen species production, destroy microbial cells. The work provides insight into the developing field of research on versatile bimetallic nanoparticles featuring improved antibacterial characteristics. Future studies could improve the synthesis parameters to increase Ag/ZnO-NPs' antibacterial effectiveness and investigate how they could be utilised in the biomedical field. This would open a path for creating innovative nanomaterials for medical and environmental applications.

Data availability

Data are available upon reasonable request.

Conflicts of interest

There are no conflicts to declare.

Acknowledgements

The authors thank Indian Science Technology and Engineering Facilities Map (I-STEM), a Program supported by the Office of the Principal Scientific Adviser to the Govt. of India, for enabling access to the field emission scanning electron microscope (FESEM) coupled with energy dispersive spectroscopy (EDS), MAIA3XMH at Sophisticated Analytical Instrument Facility (DST-SAIF), Mahatma Gandhi University, Kottayam, India, to carry out this work.

References

1 S. S. Salem, *Arch. Microbiol.*, 2023, **205**, 1–15.
2 R. Revathy, T. Sajini, C. Augustine and N. Joseph, *Results Eng.*, 2023, **18**, 101114.
3 T. R. Sreelakshmi, T. Sajini and B. Mathew, *Adv. Mater. Res.*, 2023, **1175**, 63–72.
4 L. Jiang, Y. Guo, Z. Liu and S. Chen, *Nanoscale*, 2024, **16**, 5521–5536.
5 C. Ragavendran, C. Kamaraj, D. Natarajan, K. A. Al-Ghanim, M. Magesh, M. Nicoletti and M. Govindarajan, *Green Process. Synth.*, 2023, **13**, 20230194, DOI: 10.1515/gps-2023-0194.
6 T. Sajini, S. John and B. Mathew, *Polym. Chem.*, 2019, **10**, 5364–5384.
7 T. Sajini, R. Thomas and B. Mathew, *Chin. J. Polym. Sci.*, 2019, **37**, 1305–1318.
8 K. P. Theertha, A. Tissamol, S. K. Ashok, R. Revathy and T. Sajini, *Chem. Pap.*, 2023, **78**, 1601–1611, DOI: 10.1007/s11696-023-03188-2.
9 T. Abraham, K. P. Theertha, S. K. Ashok, J. Joseph and T. Sajini, *J. Turk. Chem. Soc., Sect. A*, 2024, **11**, 981–994.
10 R. Sunil, J. Joseph and T. Sajini, *S. Afr. J. Chem.*, 2024, **78**, 192–203.

11 G. Sharma, A. Kumar, S. Sharma, M. Naushad, R. Prakash Dwivedi, Z. A. ALOthman and G. T. Mola, *J. King Saud Univ., Sci.*, 2019, **31**, 257–269.
12 M. Sharma, R. Tyagi, M. M. Srivastava and S. Srivastava, *Green Synth. Silver Nanomater.*, 2022, pp. 99–123.
13 G. Thirumoorthy, B. Balasubramanian, J. A. George, A. Nizam, P. Nagella, N. Srinatha, M. Pappuswamy, A. M. Alanazi, A. Meyyazhagan, K. R. R. Rengasamy and V. Veerappa Lakshmaiah, *Sci. Rep.*, 2024, **14**, 1–15.
14 R. Araya-Hermosilla, J. Martínez, C. Z. Loyola, S. Ramírez, S. Salazar, C. S. Henry, R. Lavín and N. Silva, *Ultrason. Sonochem.*, 2023, **99**, 106545, DOI: **10.1016/j.ultsonch.2023.106545**.
15 N. Arora, K. Thangavelu and G. N. Karanikolos, *Front. Chem.*, 2020, **8**, 1–22.
16 H. Liu and T. J. Webster, *Biomaterials*, 2007, **28**, 354–369.
17 A. H. Hashem and G. S. El-Sayyad, *Biomass Convers. Biorefin.*, 2023, 1–13, DOI: **10.1007/s13399-023-04126-8**.
18 G. M. Nair, T. Sajini and B. Mathew, *Talanta Open*, 2022, **5**, 100080.
19 R. Revathy, J. Joseph, C. Augustine and T. Sajini, *Environ. Sci.: Adv.*, 2022, **1**, 491–505.
20 M. A. Afzal, M. Javed, S. Aroob, T. Javed, M. M. Alnoman, W. Alelwani, I. Bibi, M. Sharif, M. Saleem, M. Rizwan, A. Raheel, I. Maseeh, S. A. C. Carabineiro and M. B. Taj, *Nanomaterials*, 2023, **13**, 2079, DOI: **10.3390/nano13142079**.
21 D. S. Idris, A. Roy, A. Subramanian, S. Alghamdi, K. Chidamabaram and N. F. Qusty, *J. Inorg. Organomet. Polym. Mater.*, 2023, **5**, 1908–1919, DOI: **10.1007/S10904-023-02936-X**.
22 Z. Zaheer and S. M. Albukhari, *Arabian J. Chem.*, 2020, **13**, 7921–7938.
23 M. Ehsan, A. Waheed, A. Ullah, A. Kazmi, A. Ali, N. I. Raja, Z. U. R. Mashwani, T. Sultana, N. Mustafa, M. Ikram and H. Li, *BioMed Res. Int.*, 2022, 1215183, DOI: **10.1155/2022/1215183**.
24 S. Phongtongpasuk, S. Poadang and N. Yongvanich, *Energy Procedia*, 2016, **89**, 239–247.
25 M. A. Mahdi, M. T. Mohammed, A. N. Jassim and Y. M. Taay, *J. Phys.: Conf. Ser.*, 2021, **1853**, 012039, DOI: **10.1088/1742-6596/1853/1/012039**.
26 R. Selvaraj, A. Kamalanathan, K. Padmavathy, K. Sivakumari, S. Karthika, S. Rajesh and K. Ashok, *Int. J. Pharm. Sci. Res.*, 2021, **12**, 2770–2778.
27 L. Fatiha, Z. Dwyana and E. Johannes, *Proc. 2nd Int. Conf. Educ. Technol. (ICETECH 2021)*, 2022, vol. 630, pp. 380–386.
28 S. K. R. Bassiag, K. R. Aguinaldo, Z. A. Singson and R. Guzmán, *Res. Sq.*, 2023, DOI: **10.21203/rs.3.rs-3188025/v1**.
29 C. Saenjum, T. Pattananandecha and K. Nakagawa, *Molecules*, 2021, **26**(12), 3565, DOI: **10.3390/molecules26123565**.
30 N. Nerdy and K. Manurung, *Rasayan J. Chem.*, 2018, **11**, 1183–1192.
31 M. I. Masum, M. M. Siddiqa, K. A. Ali, Y. Zhang, Y. Abdallah, E. Ibrahim, W. Qiu, C. Yan and B. Li, *Front. Microbiol.*, 2019, **10**, 1–18.
32 A. A. Sorescu, A. Nuță, R.-M. Ion and Ș. B. Ioana-Raluca, *Proc. 4th Int. Virtual Conf. Adv. Sci. Results*, 2016, vol. 4, pp. 188–193.
33 T. Sajini, S. John and B. Mathew, *J. Polym. Res.*, 2022, **29**, 509, DOI: **10.1007/s10965-022-03361-3.**
34 S. B. Aziz, O. G. Abdullah, D. R. Saber, M. A. Rasheed and H. M. Ahmed, *Int. J. Electrochem. Sci.*, 2017, **12**, 363–373.
35 R. Manikandan, B. Manikandan, T. Raman, K. Arunagirinathan, N. M. Prabhu, M. Jothi Basu, M. Perumal, S. Palanisamy and A. Munusamy, *Spectrochim. Acta, Part A*, 2015, **138**, 120–129.
36 T. Y. Suman, S. R. Radhika Rajasree, R. Ramkumar, C. Rajthilak and P. Perumal, *Spectrochim. Acta, Part A*, 2014, **118**, 11–16.
37 S. Bhattacharjee, *J. Controlled Release*, 2016, **235**, 337–351.
38 O. Pawar, N. Deshpande, S. Dagade, S. Waghmode and P. Nigam Joshi, *J. Exp. Nanosci.*, 2016, **11**, 28–37.
39 L. A. Minhas, M. Kaleem, A. Jabeen, N. Ullah, H. M. U. Farooqi, A. Kamal, F. Inam, A. F. Alrefaei, M. H. Almutairi and A. S. Mumtaz, *Microorganisms*, 2023, **11**, 1–19.
40 S. Dubey, A. Shukla and R. K. Shukla, *Curr. Chem. Lett.*, 2023, **12**, 799–812.
41 M. Hosny, M. Fawzy and A. S. Eltaweil, *Sci. Rep.*, 2022, **12**, 1–17.
42 I. Singh, T. Mazhar, V. Shrivastava and R. Singh Tomar, *Int. J. Nano Dimens.*, 2022, **13**, 168–178.
43 K. Kayed, M. Issa and E. Alsoki, *Plasmonics*, 2023, **18**, 711–717.
44 A. A. Fayyadh and M. H. Jaduaa Alzubaidy, *J. Mech. Behav. Mater.*, 2021, **30**, 228–236.
45 V. N. Jafarova and G. S. Orudzhev, *Solid State Commun.*, 2021, **325**, 114166.
46 K. Davis, R. Yarbrough, M. Froeschle, J. White and H. Rathnayake, *RSC Adv.*, 2019, **9**, 14638–14648.
47 T. Khalafi, F. Buazar and K. Ghanemi, *Sci. Rep.*, 2019, **9**, 6866, DOI: **10.1038/S41598-019-43368-3**.
48 H. D. Kyomuhimbo, I. N. Michira, E. I. Iwuoha and U. Feleni, *Processes*, 2022, **10**, 1–18.
49 M. Hosny, M. Fawzy and A. S. Eltaweil, *Sci. Rep.*, 2022, **12**, 1–17.
50 C. K. Somasundaram, R. Atchudan, T. N. J. I. Edison, S. Perumal, R. Vinodh, A. K. Sundramoorthy, R. S. Babu, M. Alagan and Y. R. Lee, *Catalysts*, 2021, **11**, 1–13.
51 J. Singh, T. Dutta, K. H. Kim, M. Rawat, P. Samddar and P. Kumar, *J. Nanobiotechnol.*, 2018, **16**, 1–24.
52 G. Maheshwaran, A. Nivedhitha Bharathi, M. Malai Selvi, M. Krishna Kumar, R. Mohan Kumar and S. Sudhahar, *J. Environ. Chem. Eng.*, 2020, **8**, 104137.
53 S. Jabeen, R. Qureshi, M. Munazir, M. Maqsood, M. Munir, S. S. H. Shah and B. Z. Rahim, *Mater. Res. Express*, 2021, **8**, 092001, DOI: **10.1088/2053-1591/AC1DE3**.
54 S. Sajjad, S. A. K. Leghari, N. U. A. Ryma and S. A. Farooqi, *Macabresque Hum. Viol. Hate Genocide, Mass Atrocity Enemy-Making*, 2018, pp. 23–77.

55 S. Alamdari, M. S. Ghamsari, C. Lee, W. Han, H. H. Park, M. J. Tafreshi, H. Afarideh and M. H. M. Ara, *Appl. Sci.*, 2020, **10**, 3620.
56 P. Basnet, T. Inakhunbi Chanu, D. Samanta and S. Chatterjee, *J. Photochem. Photobiol., B*, 2018, **183**, 201–221.
57 M. Tesfaye, Y. Gonfa, G. Tadesse, T. Temesgen and S. Periyasamy, *Heliyon*, 2023, **9**, e17356.
58 A. E. Sultan, H. I. Abdullah and A. H. Niama, *Nanomed. Res. J.*, 2023, **8**, 259–267.
59 M. Lopez-Carrizales, M. A. Pérez-Díaz, E. Mendoza-Mendoza, R. D. Peralta-Rodríguez, H. J. Ojeda-Galván, D. Portales-Pérez, M. Magaña-Aquino, R. Sánchez-Sánchez and F. Martinez-Gutierrez, *New J. Chem.*, 2022, **46**, 17841–17853.
60 B. Abebe, B. Kefale and D. T. Leku, *RSC Adv.*, 2023, **13**, 4523–4529.
61 Y. Cao, H. A. Dhahad, M. A. El-Shorbagy, H. Q. Alijani, M. Zakeri, A. Heydari, E. Bahonar, M. Slouf, M. Khatami, M. Naderifar, S. Iravani, S. Khatami and F. F. Dehkordi, *Sci. Rep.*, 2021, **11**, 1–8.
62 A. N. Sumbal, S. Naz, J. S. Ali, A. Mannan and M. Zia, *Biotechnol. Rep.*, 2019, **22**, e00338.
63 J. S. Moodley, S. B. N. Krishna, K. Pillay and P. Govender, *Adv. Nat. Sci.: Nanosci. Nanotechnol.*, 2018, **9**, 015011, DOI: **10.1088/2043-6254/aaabb2**.
64 K. Dulta, P. Chauhan, K. Thakur and P. K. Chauhan, *AIP Conf. Proc.*, 2022, **2357**, 050009, DOI: **10.1063/5.0080981**.
65 P. Banerjee, M. Satapathy, A. Mukhopahayay and P. Das, *Bioresour. Bioprocess.*, 2014, **1**, 1–10.
66 S. Ahmed, Saifullah, M. Ahmad, B. L. Swami and S. Ikram, *J. Radiat. Res. Appl. Sci.*, 2016, **9**(1), 1–7, DOI: **10.1016/j.jrras.2015.06.006**.
67 R. C. De Souza, L. U. Haberbeck, H. G. Riella, D. H. B. Ribeiro and B. A. M. Carciofi, *Braz. J. Chem. Eng.*, 2019, **36**, 885–893.
68 H. Ashraf, T. Anjum, S. Riaz and S. Naseem, *Front. Microbiol.*, 2020, **11**, 1–22.
69 H. R. Rajabi, R. Naghiha, M. Kheirizadeh, H. Sadatfaraji, A. Mirzaei and Z. M. Alvand, *Mater. Sci. Eng., C*, 2017, **78**, 1109–1118.
70 C. Liao, Y. Li and S. C. Tjong, *Int. J. Mol. Sci.*, 2019, **20**(2), 449, DOI: **10.3390/ijms20020449**.
71 N. M. Alabdallah and M. M. Hasan, *Saudi J. Biol. Sci.*, 2021, **28**, 5631–5639.